Applied Physics Letters ARTICLE pubs.aip.org/aip/apl

Electromechanical switching in DNA–CNT supramolecular structures

Cite as: Appl. Phys. Lett. **127**, 023505 (2025); doi: 10.1063/5.0272693
Submitted: 26 March 2025 · Accepted: 27 June 2025 ·
Published Online: 15 July 2025

View Online Export Citation CrossMark

Olaiyan Alolaiyan,[1,2,a)] Arpan De,[1] and M. P. Anantram[1]

AFFILIATIONS

[1]Department of Electrical and Computer Engineering, University of Washington, Seattle, Washington 98195, USA
[2]Center of Excellence for Green Nanotechnologies, Microelectronics and Semiconductor Institute, King Abdulaziz City for Science and Technology, Riyadh 11442, Saudi Arabia

[a)]Author to whom correspondence should be addressed: olaiyan@uw.edu

ABSTRACT

The characteristics of the interface between DNA and metallic carbon nanotube (CNT) in supramolecular assemblies are important to understand for electronic and sensing applications. We study the mechanical stability and electronic properties of these interfaces with amino and ester linkers using computational experiments. Our study demonstrates that both linkers significantly enhance the mechanical stability of DNA–CNT systems, with the DNA adopting a stable and lower energy perpendicular orientation relative to the CNT as opposed to a conventional parallel arrangement. This lower energy configuration is driven by nonbonded interactions between the DNA base and the CNT surface. Our calculations also reveal that interface resistance is primarily governed by DNA–CNT interactions with negligible contribution from the linkers. In the case of the amino linker, we predict a 100-fold transmission ratio between parallel and perpendicular configurations of DNA relative to CNT. This observation can be used to build an electromechanical switch with fast switching times (30 ns). The ester linker, on the contrary, enables a better electronic coupling between the DNA and CNT even when strained.

Published under an exclusive license by AIP Publishing. https://doi.org/10.1063/5.0272693

Programmability, scalability, and power efficiency are key factors that make DNA-based nanotechnology a promising alternative to advanced solid-state devices and circuits. Over the past few decades, DNA nanotechnology has made significant strides, primarily owing to the self-assembly capabilities of DNA. This has enabled the construction of supramolecular structures, such as origami[1–4] and tiles,[5,6] which are useful for nanoscale patterning and assembly and doping in silicon.[7–10] Additionally, DNA origami has been employed for site-specific doping to control the electronic properties of these structures. There is a growing interest in modifying the intrinsic properties of DNA to develop nanoelectronic devices and circuits where DNA serves as the conducting channel. However, bridging the gap between DNA nanotechnology and mainstream electronics requires advancements on two major fronts: (i) engineering the intrinsic electronic properties of DNA and (ii) establishing strong, low-resistance electrical contacts to DNA.

Efforts to improve electrical conductance have involved using multiple DNA nanostructures to create superlattice or heterostructure devices.[11,12] Research has also shown that altering DNA conformation[13] or stretching[14] the DNA can significantly enhance electrical conductance. Furthermore, intercalating DNA with organic molecules such as anthraquinone[15] or heavy metal atoms[16] reduces the bandgap and increases conductance.

Connecting DNA to metallic contacts where voltages are applied remains a challenging issue.[17,18] These interfaces should be mechanically stable and electrically conductive. Strong covalently bonded linkers are needed for mechanical strength, but they tend to be resistive.[19–22] Bonding between conventional metals and DNA is the norm, but these contacts are not mechanically stable, and they suffer from noise in measured conductance. It is known that the conductive path through the DNA is primarily through the bases, and the question remains if there is an effective way to tap into the pi orbitals at the bases using a metallic contact. One promising solution is to connect DNA to metallic carbon nanotubes (CNTs),[23,24] which offer mechanically strong contacts via covalent bonding. Additionally, the pi electrons on the CNT may be leveraged to increase the conductivity. The established chemistry between DNA and CNTs[25] lends support to this proposition, thereby creating opportunities for the development of scalable molecular circuits.

Additional studies affirm the potential of DNA–CNT interfaces for nanoelectronic applications. Covalently bonded DNA–CNT junctions have been demonstrated to exhibit stable and reversible

Published under an exclusive license by AIP Publishing

conductivity, which addresses some limitations of conventional metal–DNA contacts.[26] Simulation results indicate that the binding configuration and conformational dynamics at the DNA–CNT interface are critical for effective electronic coupling.[27,28] In aqueous environments, linker-induced assembly produces reliable CNT junctions with enhanced mechanical stability,[29] while chemical modifications at the interface, such as protonation, can be employed to fine-tune the electronic properties.[30]

Motivated by the experimental feasibility of engineering DNA–CNT contacts, this work focuses on studying the interface between CNTs and DNA using computational simulations. We use molecular dynamics simulations over extended timescales and density functional theory-based electronic structure calculations to investigate the interactions between DNA and two types of linker molecules: amino-based and ester-based. The amino linker has been previously used experimentally,[23,24,31] but the physical behavior of the interface remains largely unexplored. Our simulations suggest that the amino linker could enable significant electromechanical switching. The ester linker, though less common, may offer advantages, as we observe that the transmission of structures using this linker is less sensitive to strain. Furthermore, we show that both linkers provide a robust way to couple the pi electrons of the CNT to those in the DNA bases.

We consider a DNA sequence, 5′-GGGCCCGGGCCC-3′, which is covalently attached to a metallic carbon nanotube (CNT) via either an amino or ester linker (Fig. S1). The DNA is modeled using the bsc1 force field,[32] while the CNT is modeled using the General Amber Force Field (GAFF) with partial charges determined from previous studies.[33–37] We perform calculations with eleven (11) and twenty-two (22) metallic CNT unit cells. We propose that these key observations are broadly applicable across all canonical DNA motifs. Moreover, the perpendicular orientation of DNA with respect to CNT has been tested for an extended time window (1.1 μs) for both amino- and ester linkers (see Fig. S8).

The 10-atom amino chain linker considered consists of an amine group (-NH_2), followed by a pair of carbonyl groups (−C = O), a hexamethylene spacer (−$(CH2)_6$−), and a carboxyl group (−COOH) at the terminus (see Fig. S1). The carboxyl group was incorporated to facilitate attachment to the CNT. This linker was selected because it makes stable bonds to the 2′ position of DNA sugars, which is essential for DNA–CNT conjugation. We calculated the partial charges in the linker by first optimizing its structure using density functional theory (DFT) with the B3LYP functional and a 6–31G* basis set in Gaussian 16.[38] Following optimization, we obtained the partial charges using the Hartree-Fock method with a 6–31G* basis set. The charge distribution was further refined using the Merz–Kollman (MK) population analysis, followed by RESP fitting.[39] The resulting RESP-derived charges were incorporated into the force field parameters, ensuring compatibility with the GAFF framework. A similar procedure was followed for the ester-based linker.

In the next step, we attach the amino linker to the DNA by removing one hydrogen atom from the 2′-deoxyribose sugar of the DNA and one hydrogen atom from the amino group (-NH_2) of the linker, thereby enabling the formation of a bond between the DNA and linker. This leads to an (-NH) group at the linker's terminal [see Figs. S1(c) and S1(d)]. Similarly, on the CNT side, we remove one hydrogen atom from a terminal carbon of the CNT and one hydrogen atom from the carboxyl group (-COOH) of the linker to form a direct carbon–carboxyl (C–COO) bond. To maintain charge neutrality in the resulting DNA–linker–CNT (DLC) complex, we redistribute the partial charges by assigning the removed charges to the nearest hydrogen atoms at the new bond sites. For the ester linker, a similar approach was used. We removed a hydrogen atom from the 3' hydroxyl group of the sugar in DNA and bonded it with the carbonyl carbon atom of the ester [see Fig. S1(e)]. The DLC structure is solvated using an octahedral water box (15 Å cutoff) containing TIP3P water molecules and 22 sodium counterions (Na^+) to neutralize the system. After energy minimization, we heat (NVT) and equilibrate (NPT) for 1 ns each with a target temperature of 300 K using the Langevin thermostat and the SHAKE algorithm. Finally, we performed a production run for 100 ns. This run started from the equilibrated structure and velocities and was carried out under the NPT ensemble. The MD procedure developed for this study is discussed in detail in the supplementary material, and the calculated partial charge on each atom for both the amino and ester linkers is presented in Tables S1 and S2 of the supplementary material.

From the 100 000 MD frames, we performed structural clustering and identified the dominant configurations, parallel and perpendicular, based on population. The centroid structures of these clusters were used as representative geometries for DFT and transport calculations. We carry out DFT calculations using the B3LYP exchange–correlation functional and the 6–31G(d,p) basis set with the polarizable continuum model. The Fock (F) and Overlap (S) matrices from the DFT calculations are used to obtain a Hamiltonian (H) in an orthogonal basis,

$$H = S^{-\frac{1}{2}} F S^{-\frac{1}{2}}. \tag{1}$$

The retarded Green's function (G^r) is calculated from Refs. 15 and 40

$$[E - (H + \Sigma_{CNT} + \Sigma_{TC} + \Sigma_B)]G^r = I. \tag{2}$$

The transmission T_{eff} is calculated using[40]

$$T_{eff} = T_{CNT,TC} + \sum_{i=1}^{N_b} \sum_{j=1}^{N_b} T_{CNT,i} W_{ij}^{-1} T_{j,TC}, \tag{3}$$

where W_{ij}^{-1} is the inverse of the matrix $W_{ij} = [(1 - R_{ii}) \times \delta_{ij} - T_{ij}(1 - \delta_{ij})]$, R_{ii} is the reflection at probe i, and T_{ij} is the transmission from probe i to j. $T_{CNT,TC}$ is the direct transmission between the CNT end and top contact in Figs. 2(a) and 2(b), and the second term represents the decoherence contribution to the transmission via decoherence probes. N_b is the total number of decoherence probes.

The density of states (DOS) at atom m is calculated by summing over the diagonal components ($G^r_{m,i}$) of the retarded Green's function corresponding to orbital i on atom m using

$$DOS(m, E) = -\frac{1}{\pi} \sum_i Im\left(G^r_{m,i}(E)\right). \tag{4}$$

We consider a carbon nanotube connected to DNA via either an amino (long) or ester (short) linkers. The longer linker was chosen because of well-established reaction pathways that have been utilized experimentally. While it seems plausible that the flexibility of a long linker will make it possible to have multiple configurations at room temperature, we find that the interactions between the DNA and carbon nanotube help to stabilize the configuration. The shorter linker was chosen with the thought that the energy barrier from the carbon nanotube to the linker is shorter, thus increasing the tunneling probability between them. To establish the physics of electron transport at

Published under an exclusive license by AIP Publishing

this interface, it is important to perform molecular dynamics (MD) simulations and cluster the resulting configurations, providing insight into the relative probabilities of various atomic configurations. We choose the metallic (6,6) carbon nanotube whose lateral dimensions are comparable to those of the DNA.

We model the systems from an initial state where the carbon nanotube is parallel to DNA, as shown in Fig. 1, where the purple and red lines represent the orientation of the CNT and DNA, respectively. The sequence in Figs. 1(a) and 1(b) illustrates the evolution of the configuration with amino and ester linkers from the initial (0 ns) to the final time (100 ns). The time evolution in the case of both linkers shows a few common features in how the structures reorganize with time. At 0 ns, the DNA and CNT are aligned along a line with the angle between them being $\sim 180^\circ$, and this is referred to as the parallel configuration [Fig. 1(a)] With time, the DNA, while remaining nearly rigid, bends at the linker. Finally, after $\sim$30 ns, the DNA orients at an angle close to 90° with respect to the CNT, assuming a perpendicular configuration [Fig. 1(a)]. This conformation is stable and persists for the remainder of the simulation period. To support this observation, we calculated the potential energy and found that the perpendicular configuration is energetically more favorable, with energy of 2920.15 kcal/mol compared to 2977.36 kcal/mol for the parallel case. A similar trend is observed in the case with an ester linker [Fig. 1(b)]. These observations are robust and observed in simulations involving both 11 and 22 unit cells of the CNT. Furthermore, we observed that for the shorter CNT, the structure persists for 1 μs and is realized for a variety of initial configurations.

To evaluate the stability of the resulting configurations, we analyze the root mean square deviation (RMSD) between the coordinates of 100 000 frames, equally spaced over the 100 ns simulation time, using two-dimensional RMSD plots. These 2D plots compare each frame against every other frame, where the y axis shows the reference frame, and the x axis shows the frame being compared. The color corresponds to the RMSD value, as shown in the scale bar. The diagonal line represents the self-comparison of frames, and darker blue points indicate structural similarity, which reflects stability. For the DNA–CNT supramolecular structure, the RMSD is approximately 6 Å without a linker, as shown in Fig. 1(c). In comparison, the structures with linkers have a considerably smaller RMSD of 3.5 Å (amino) and 2.5 Å (ester), thus elucidating the importance of the linker in stabilizing the DNA–CNT system [see Figs. 1(d) and 1(e)]. From the MD simulation trajectory, we observe that for the amino linker, the transition of the DNA from a parallel to a perpendicular orientation relative to the CNT occurs at around 30 ns, at which point the RMSD decreases below 6 Å [Fig. 1(d)]. Similarly, with an ester linker, RMSD values are

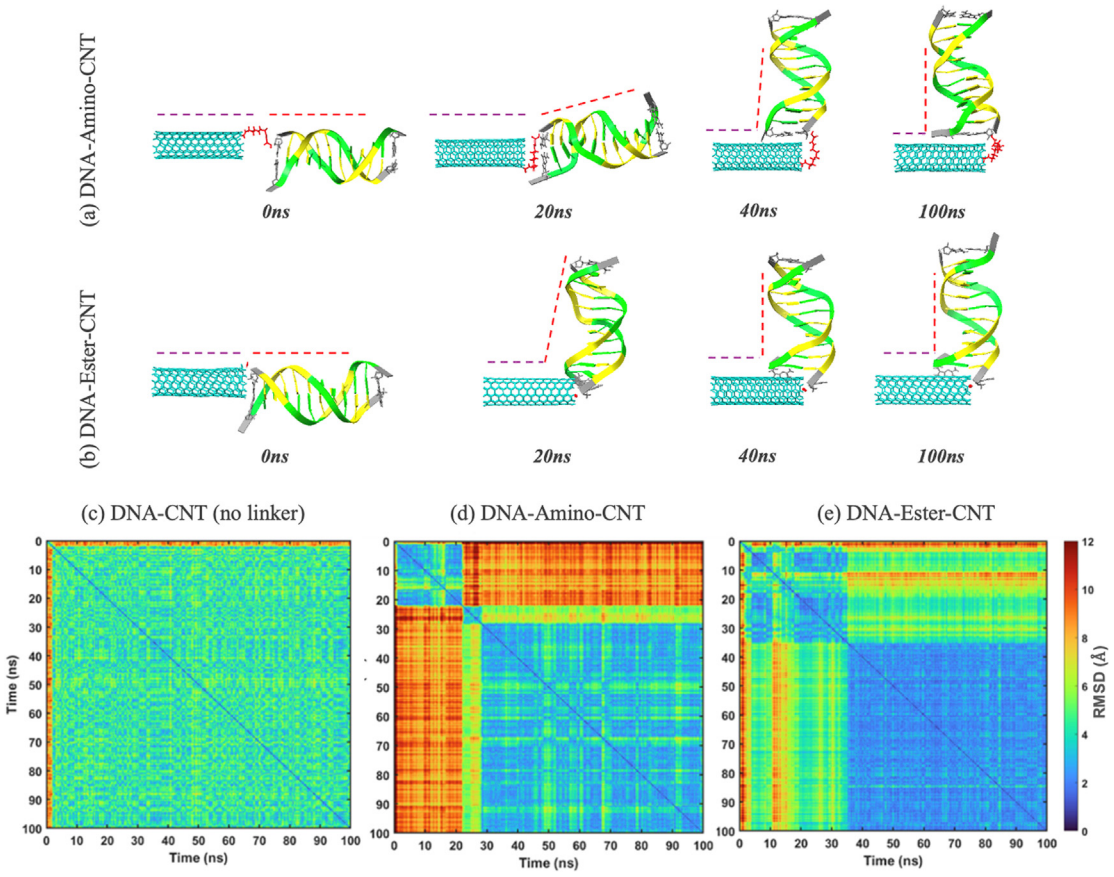


FIG. 1. (Molecular dynamics results for DNA–linker–CNT system): Time evolution of the system-under-study from 0 to 100 ns with (a) amino linker and (b) ester linker. 2D RMSD heatmaps for (c) DNA–CNT (no linker), DNA–CNT with (d) amino and (e) ester linkers over the 100 ns simulation time. The purple dotted lines in (a) and (b) represent the orientation of the CNT while the red dotted lines are representative of the orientation of the DNA. The crimson-colored molecule in both (a) and (b) is the linker.

Published under an exclusive license by AIP Publishing

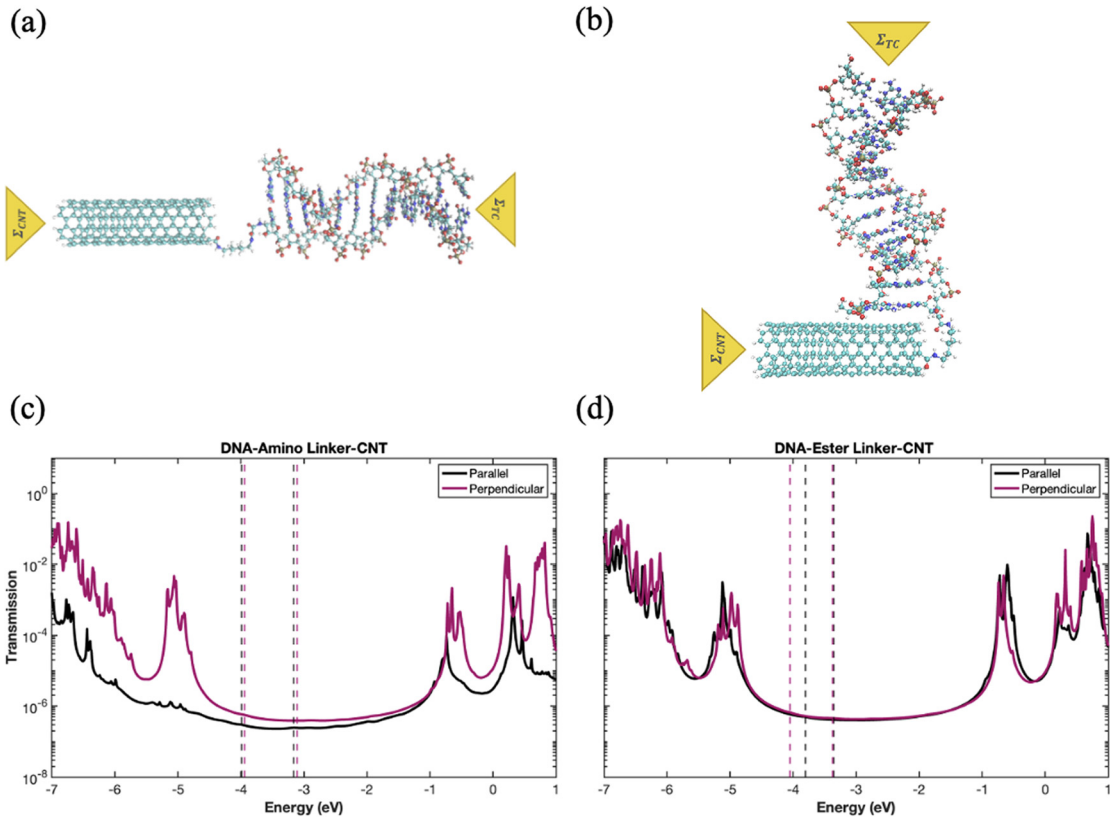


FIG. 2. (Transport profiles for DNA–linker–CNT systems): Configurations for the transport calculations of DNA–CNT systems with amino and ester linkers are shown at two different time points: (a) 0 ns (parallel configuration with injection/extraction sites) and (b) 100 ns (perpendicular configuration with injection/extraction sites). The corresponding transport profiles as a function of energy are presented in (c) and (d). In panels (c) and (d), the dotted lines indicate the HOMO and LUMO levels of the entire system.

below 4 Å after ∼35 ns, when the system assumes a perpendicular configuration. From the RMSD 2D map in Figs. 1(d) and 1(e), we conclude that the ester linker is more stable compared to the amino linker, with the DNA adopting a perpendicular orientation that is maintained throughout the simulation. This observation is also confirmed in the atom-wise RMSF (root mean square fluctuations) shown in Figs. S2 and S5. We tested the robustness of this transition by running additional simulations with varied initial configurations and random seeds. In all cases, the DNA adopted a perpendicular orientation, with transition times ranging from 2 to 30 ns (see Fig. S6).

In the next step, we study the physics of electronic transport from CNT to DNA across the linker. We clustered the 100,000 conformations obtained from MD simulations and extracted the central motif of all clusters for charge transport calculations. We calculate the off diagonal Green's function of the supramolecular structure and then relate this to the electron transmission across the entire structure. For this, the Hamiltonian and overlap matrices of the CNT are obtained from the density functional theory calculations. This procedure provides an accurate way to model the interface between the CNT and DNA in a non-perturbative manner. We attach probes to the atoms to account for decoherence effects. Finally, using Green's function approach, the electron transmission probability is summed over all modes, and the transmission is calculated using Eq. (3).

We find that the electron transmission at the HOMO energies of the DNA increases by almost 500 times when DNA changes orientation from parallel to perpendicular relative to the CNT (Fig. 2). In the perpendicular orientation, the pi-orbital overlap between the CNT and DNA atoms is significantly larger because they self-assemble to an inter-graphitic distance of 3.4 Å. This causes a strong overlap between the wavefunctions of DNA and CNT in the perpendicular configuration, whereas there is no wavefunction overlap in the parallel configuration. Close-up views of the DNA–CNT interface are shown in Fig. S7. To demonstrate this, we show the HOMO to HOMO-4 orbitals in Fig. 3. In the parallel configuration, the orbitals are localized on the DNA and CNT without them overlapping. In the perpendicular configuration, we observe marked delocalization of the orbitals, where the orbitals on the DNA and CNT directly overlap, with the linker simply acting as a bridging component. As a result, while in the perpendicular configuration, electrons can travel directly from the CNT to DNA; in the parallel configuration, electrons must travel through the covalently bonded linker atoms. This is the underlying reason for the low transmission. Applying a force to induce a relative separation between the DNA and CNT should result in a significant change in conductance that would be experimentally observable. In the case of the ester linker also, there is a large increase in transmission through the HOMO energies of the DNA when the orientation transitions from parallel to

Published under an exclusive license by AIP Publishing

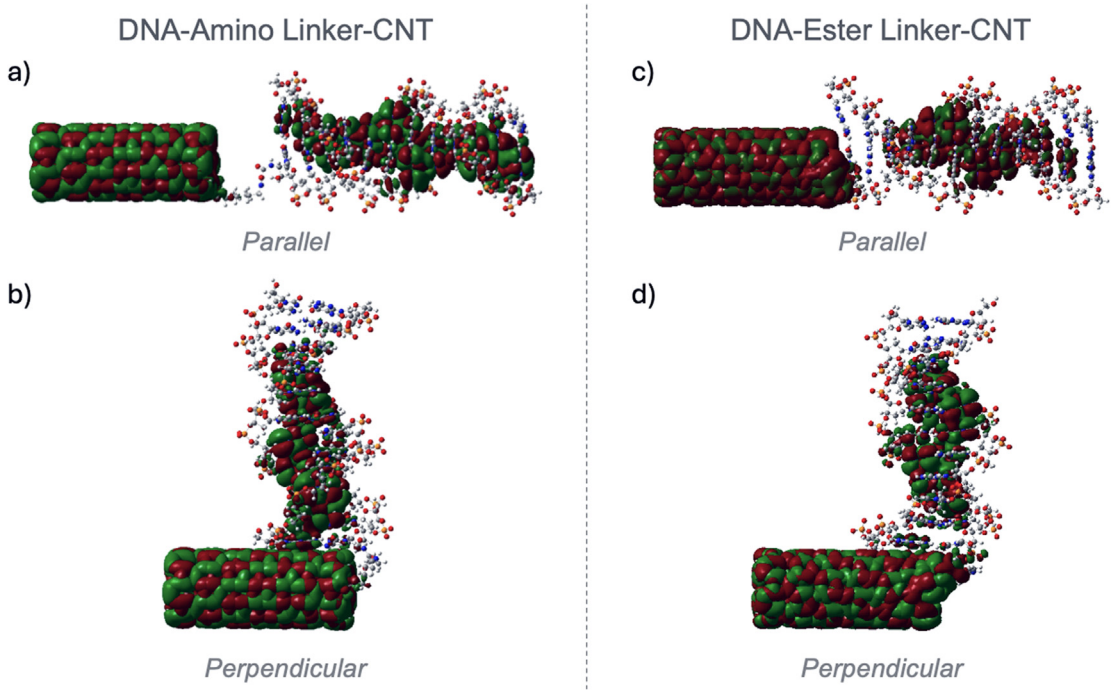


FIG. 3. (The wavefunctions for DNA–linker–CNT systems): (a) Initial (parallel) and (b) Final (perpendicular) structures for DNA–amino linker–CNT, displaying the combined wavefunctions for HOMO to HOMO-4 with an iso value of 0.002. Similarly, (c) initial (parallel) and (d) final (perpendicular) structures for DNA–ester linker–CNT.

perpendicular, though it is not as large as the amino case (16 times increase). As the ester linker length is smaller than the amino linker length in the parallel configuration, our calculations show that the tunneling probability is higher. This leads to a smaller change in transmission between the perpendicular and parallel conformations in the ester linker compared to the amino linker.

We also calculated the density of states (DOS) for both conformations and showed the larger DOS available for hopping directly from CNT to DNA. The DOS for the CNT and DNA in parallel configuration are separated by the linker, which has a small DOS, which makes transport difficult (Fig. S3). In contrast, in the perpendicular configuration, the proximity of the large DOS on both the CNT and DNA helps in tunneling across the interface, bypassing the linker, which has a low DOS at these energies (Fig. S4). These observations are put on a firmer mathematical footing by calculating the transmission probability across the supramolecular structure by selectively turning off the ability of an electron to travel through the linker. Specifically, in terms of conduction pathways, there are two possible choices: first, conduction from CNT to DNA via the linker, and second, direct transport between CNT and DNA bypassing the linker. To probe the contribution of each of these pathways, we set the Hamiltonian between (i) the DNA and CNT to zero, $H_{CNT-DNA} = 0$, thus, forcing the electronic transport to happen only through the linker, and (ii) both the DNA and linker and the CNT and linker to zero, $H_{DNA-Linker} = 0$ and $H_{CNT-Linker} = 0$, thus, forcing the conduction to occur only by direct hopping between CNT and DNA. The transmission profiles computed on the original Hamiltonian are shown in Figs. 4(a) and 4(d) for amino and ester linkers, respectively. When we modify the Hamiltonian such that the coupling between DNA and CNT is turned off ($H_{CNT-DNA} = 0$), the transmission drops significantly, as evident from Figs. 4(b) and 4(e). In contrast, turning off the coupling between DNA–linker and CNT–linker ($H_{DNA-Linker} = 0$ and $H_{CNT-Linker} = 0$) does not affect the transmission significantly. Additionally, we analyzed the transmission at the HOMO of DNA (−4.88 eV) for each case. In the amino linker case, $H_{CNT-DNA} = 0$ [Fig. 4(b)], we observe a 150-fold drop in transmission from the original Hamiltonian [Fig. 4(a)]. In contrast, turning off the linker coupling results in almost no change in the transmission [Fig. 4(c)]. Similarly, in the ester linker case, making $H_{CNT-DNA} = 0$ reduces the transmission by 100 times [Fig. 4(e)]. However, turning off linker coupling does not change the transmission significantly [Fig. 4(f)]. These results clearly point to the dominance of DNA–CNT interaction in the overall charge transport of these supramolecules. Finally, we stress again that while the linker adds to the mechanical stability of the system, it plays a minimal role in the electronic transport through the DNA–CNT complexes.

We have modeled both the stability and electronic transport of a system comprising DNA connected to a metallic carbon nanotube via linkers using a combination of molecular dynamics and Green's function calculations. We identify stable low-energy configurations in which electronic transport can be enhanced. Our molecular dynamics calculations reveal that the low-energy configuration corresponds to a carbon nanotube and DNA assuming a perpendicular relative orientation. In this configuration, while the covalently bonded linker provides mechanical stability, it is further enhanced by direct pi–pi interactions between the metallic nanotube and DNA. These observations hold for both the amino (long) and ester (short) linkers. We find that while the linker is important in stabilizing the supramolecular structure, its impact on electron transport is nominal compared to the

Published under an exclusive license by AIP Publishing

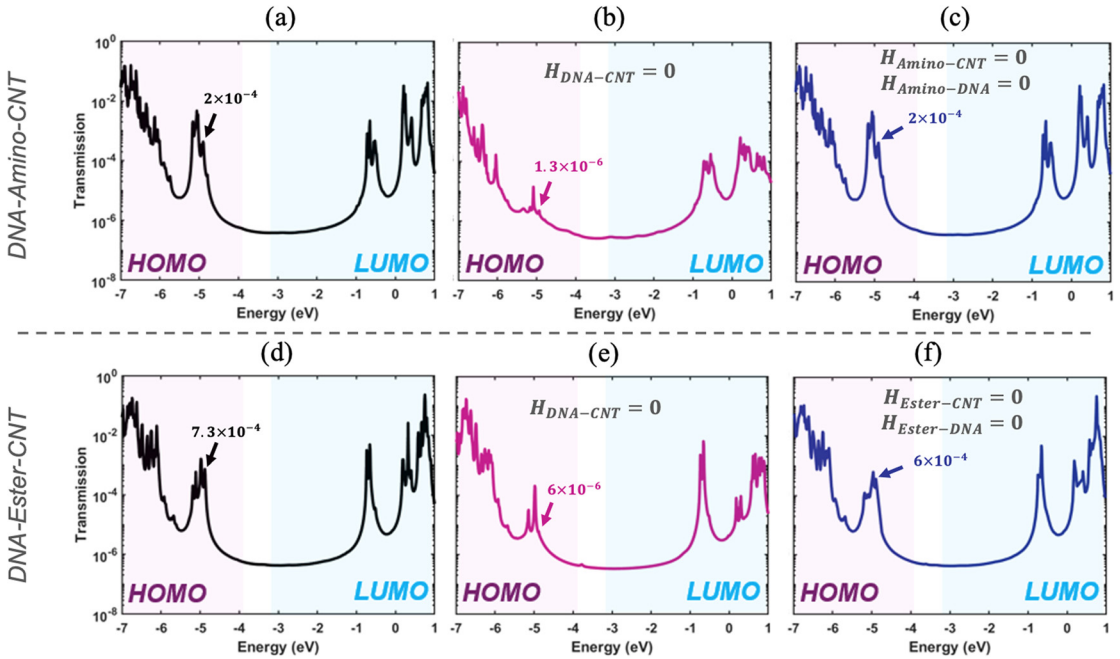


FIG. 4. (Impact of coupling between components): Transmission profiles for the DNA–CNT system are presented for two types of linkers. For the amino linker case, panels (a)–(c) display the results using the original Hamiltonian, the modified Hamiltonian with the coupling between DNA and CNT turned off, and the modified Hamiltonian with the couplings between the DNA and Linker and the CNT and Linker turned off, respectively. Similarly, for the ester linker case, panels (d)–(f) show the corresponding transmission profiles.

direct pi–orbital interactions between the DNA and CNT. A result of our calculation is the prediction of a high degree of sensitivity of electron transmission from the CNT to the DNA to the relative orientation of the two components. When the DNA transitions from a parallel to a perpendicular (more stable) orientation relative to the CNT, electron transmission probability increases dramatically–by nearly 500 times at the highest occupied molecular orbital energies of the DNA (Fig. 2). This large increase in transmission probability is attributed to the enhanced pi-orbital overlap between the CNT and DNA, which facilitates direct electron hopping between the DNA and CNT, bypassing the linker. Conversely, in the parallel configuration, the electron must travel through the linker, resulting in much lower transmission. Our simulations show it would be possible to observe electromechanical switching where the transmission is modulated by ∼100 times reversibly between the parallel and perpendicular orientations. We demonstrate using molecular dynamics simulations that the switching time from low to high transmission can be as small as 30 ns (Fig. 1), which is the time required to transition from the parallel to the perpendicular configuration. Our calculations further show that the shorter ester linker increases the tunneling probability compared to the amino linker in the parallel configuration. Consequently, we find that the amino linker provides a stronger change in resistance as the system undergoes reorientation during electromechanical switching.

See the supplementary material for a detailed description of the simulation methods, partial charge calculations, additional RMSF and DOS analyses, comparisons across different DNA orientations, close-up views of the DNA–CNT interface, extended MD simulation results, and the atomic coordinates used in both charge transport and DFT calculations.

We would like to acknowledge NSF FMSG Award No. 2229131 and NSF FMRG Award No. 2328217. OA further acknowledges King Abdulaziz City for the Science and Technology fellowship. We acknowledge using the Hyak supercomputer system at the University of Washington and thank the Research Computing Club for providing access to STF supported nodes. MPA acknowledges Manjari M-G Anant (JHU) for suggesting the use of the ester linker adopted in this work. We thank Krishna Kant Vishwakarma for useful discussions.

AUTHOR DECLARATIONS

Conflict of Interest

The authors have no conflicts to disclose.

Author Contributions

Olaiyan Alolaiyan: Data curation (equal); Formal analysis (equal); Funding acquistion (equal); Investigation (equal); Methodology (equal); Software (equal); Visualization (equal); Writing – original draft (equal); Writing – review & editing (equal). **Arpan De:** Formal analysis (equal); Validation (equal); Writing – review & editing (equal). **M. P. Anantram:** Conceptualization (equal); Funding acquistion (equal); Methodology (equal); Supervision (equal); Writing – review & editing (equal).

Published under an exclusive license by AIP Publishing

DATA AVAILABILITY

The data that support the findings of this study are available within the article and its supplementary material.

REFERENCES

[1]B. R. Madhanagopal, S. Zhang, E. Demirel, H. Wady, and A. R. Chandrasekaran, "DNA nanocarriers: Programmed to deliver," Trends Biochem. Sci. **43**(12), 997–1013 (2018).

[2]P. W. K. Rothemund, "Folding DNA to create nanoscale shapes and patterns," Nature **440**(7082), 297–302 (2006).

[3]G. Tikhomirov, P. Petersen, and L. Qian, "Fractal assembly of micrometre-scale DNA origami arrays with arbitrary patterns," Nature **552**(7683), 67–71 (2017).

[4]D. Han, X. Qi, C. Myhrvold, B. Wang, M. Dai, S. Jiang, M. Bates, Y. Liu, B. An, F. Zhang, H. Yan, and P. Yin, "Single-stranded DNA and RNA origami," Science **358**(6369), eaao2648 (2017).

[5]Y. Ke, L. L. Ong, W. M. Shih, and P. Yin, "Three-dimensional structures self-assembled from DNA bricks," Science **338**(6111), 1177–1183 (2012).

[6]L. Hui, R. Bai, and H. Liu, "DNA-based nanofabrication for nanoelectronics," Adv. Funct. Mater. **32**(16), 2112331 (2022).

[7]D. Mao, L. Liu, C. Zhang, H. Liu, and C. Mao, "Molecular lithography on silicon wafers guided by porous, extended arrays of small DNA tiles," Langmuir **39**(33), 11782–11787 (2023).

[8]L. Hui, C. Chen, M. A. Kim, and H. Liu, "Fabrication of DNA-templated Pt nanostructures by area-selective atomic layer deposition," ACS Appl. Mater. Interfaces **14**(14), 16538–16545 (2022).

[9]R. Bai, Y. Du, A. Xu, Y. Hu, J. R. Erickson, L. Hui, J. Chen, F. Xiong, and H. Liu, "DNA-based strategies for site-specific doping," Adv. Funct. Mater. **31**(1), 2005940 (2021).

[10]L. Hui, R. Nixon, N. Tolman, J. Mukai, R. Bai, R. Wang, and H. Liu, "Area-selective atomic layer deposition of metal oxides on DNA nanostructures and its applications," ACS Nano **14**(10), 13047–13055 (2020).

[11]Y. Suzuki, M. Endo, and H. Sugiyama, "Lipid-bilayer-assisted two-dimensional self-assembly of DNA origami nanostructures," Nat. Commun. **6**(1), 8052 (2015).

[12]A. Aghebat Rafat, T. Pirzer, M. B. Scheible, A. Kostina, and F. C. Simmel, "Surface-assisted large-scale ordering of DNA origami tiles," Angew. Chem., Int. Ed. **53**(29), 7665–7668 (2014).

[13]J. M. Artés, Y. Li, J. Qi, M. P. Anantram, and J. Hihath, "Conformational gating of DNA conductance," Nat. Commun. **6**(1), 8870 (2015).

[14]S. Bag, S. Mogurampelly, W. A. Goddard III, and P. K. Maiti, "Dramatic changes in DNA conductance with stretching: Structural polymorphism at a critical extension," Nanoscale **8**(35), 16044–16052 (2016).

[15]H. Mohammad, B. Demir, C. Akin, B. Luan, J. Hihath, E. E. Oren, and M. P. Anantram, "Role of intercalation in the electrical properties of nucleic acids for use in molecular electronics," Nanoscale Horiz. **6**(8), 651–660 (2021).

[16]S. Vecchioni, B. Lu, W. Livernois, Y. P. Ohayon, J. B. Yoder, C. Yang, K. Woloszyn, W. Bernfeld, M. P. Anantram, J. W. Canary, W. A. Hendrickson, L. J. Rothschild, C. Mao, S. J. Wind, N. C. Seeman, and R. Sha, "Metal-mediated DNA nanotechnology in 3D: Structural library by templated diffraction," Adv. Mater. **35**(29), 2210938 (2023).

[17]K. L. Jiménez-Monroy, N. Renaud, J. Drijkoningen, D. Cortens, K. Schouteden, C. Van Haesendonck, W. J. Guedens, J. V. Manca, L. D. A. Siebbeles, F. C. Grozema, and P. H. Wagner, "High electronic conductance through double-helix DNA molecules with fullerene anchoring groups," J. Phys. Chem. A **121**(6), 1182–1188 (2017).

[18]B. Zhang, W. Song, P. Pang, H. Lai, Q. Chen, P. Zhang, and S. Lindsay, "Role of contacts in long-range protein conductance," Proc. Natl. Acad. Sci. U. S. A. **116**(13), 5886–5891 (2019).

[19]K. Wang, "DNA-based single-molecule electronics: From concept to function," JFB. **9**(1), 8 (2018).

[20]C. Jia, B. Ma, N. Xin, and X. Guo, "Carbon electrode–molecule junctions: A reliable platform for molecular electronics," Acc. Chem. Res. **48**(9), 2565–2575 (2015).

[21]X. Dai, Q. Li, A. Aldalbahi, L. Wang, C. Fan, and X. Liu, "DNA-based fabrication for nanoelectronics," Nano Lett. **20**(8), 5604–5615 (2020).

[22]X. Guo, J. P. Small, J. E. Klare, Y. Wang, M. S. Purewal, I. W. Tam, B. H. Hong, R. Caldwell, L. Huang, S. O'Brien, J. Yan, R. Breslow, S. J. Wind, J. Hone, P. Kim, and C. Nuckolls, "Covalently bridging gaps in single-walled carbon nanotubes with conducting molecules," Science **311**(5759), 356–359 (2006).

[23]X. Guo, A. A. Gorodetsky, J. Hone, J. K. Barton, and C. Nuckolls, "Conductivity of a single DNA duplex bridging a carbon nanotube gap," Nat. Nanotechnol. **3**(3), 163–167 (2008).

[24]S. Roy, H. Vedala, A. D. Roy, D. Kim, M. Doud, K. Mathee, H. Shin, N. Shimamoto, V. Prasad, and W. Choi, "Direct electrical measurements on single-molecule genomic DNA using single-walled carbon nanotubes," Nano Lett. **8**(1), 26–30 (2008).

[25]A. D. Bobadilla and J. M. Seminario, "DNA−CNT interactions and gating mechanism using MD and DFT," J. Phys. Chem. C **115**(8), 3466–3474 (2011).

[26]C. Jia, A. Migliore, N. Xin, S. Huang, J. Wang, Q. Yang, S. Wang, H. Chen, D. Wang, B. Feng, Z. Liu, G. Zhang, D.-H. Qu, H. Tian, M. A. Ratner, H. Q. Xu, A. Nitzan, and X. Guo, "Covalently bonded single-molecule junctions with stable and reversible photoswitched conductivity," Science **352**(6292), 1443–1445 (2016).

[27]H. Gao and Y. Kong, "Simulation of DNA-nanotube interactions," Annu. Rev. Mater. Res. **34**(1), 123–150 (2004).

[28]B. Tan, M. Hodak, W. Lu, and J. Bernholc, "Charge transport in DNA nanowires connected to carbon nanotubes," Phys. Rev. B **92**(7), 075429 (2015).

[29]M. Palma, W. Wang, E. Penzo, J. Brathwaite, M. Zheng, J. Hone, C. Nuckolls, and S. J. Wind, "Controlled formation of carbon nanotube junctions via linker-induced assembly in aqueous solution," J. Am. Chem. Soc. **135**(23), 8440–8443 (2013).

[30]P. Wojton, P. Wolski, K. Wolinski, and T. Panczyk, "Protonation of cytosine-rich telomeric DNA fragments by carboxylated carbon nanotubes: Insights from computational studies," J. Phys. Chem. B **125**(21), 5526–5536 (2021).

[31]B. Liu, B. Demir, C. A. Gultakti, J. Marrs, Y. Gong, R. Li, E. E. Oren, and J. Hihath, "Self-aligning nanojunctions for integrated single-molecule circuits," ACS Nano **18**(6), 4972–4980 (2024).

[32]I. Ivani, P. D. Dans, A. Noy, A. Pérez, I. Faustino, A. Hospital, J. Walther, P. Andrio, R. Goñi, A. Balaceanu, G. Portella, F. Battistini, J. L. Gelpí, C. González, M. Vendruscolo, C. A. Laughton, S. A. Harris, D. A. Case, and M. Orozco, "Parmbsc1: A refined force field for DNA simulations," Nat. Methods **13**(1), 55–58 (2016).

[33]J. Wang, R. M. Wolf, J. W. Caldwell, P. A. Kollman, and D. A. Case, "Development and testing of a general Amber force field," J. Comput. Chem. **25**(9), 1157–1174 (2004).

[34]D. A. Case, K. Belfon, I. Y. Ben-Shalom, S. R. Brozell, D. S. Cerutti, T. E. Cheatham, V. W. D. Cruzeiro III, T. A. Darden, R. E. Duke, G. Giambasu, M. K. Gilson, H. Gohlke, A. W. Goetz, R. Harris, S. Izadi, S. A. Izmailov, K. Kasavajhala, A. Kovalenko, R. Krasny, T. Kurtzman, T. S. Lee, S. LeGrand, P. Li, C. Lin, J. Liu, T. Luchko, R. Luo, V. Man, K. M. Merz, Y. Miao, O. Mikhailovskii, G. Monard, H. Nguyen, A. Onufriev, F. Pan, S. Pantano, R. Qi, D. R. Roe, A. Roitberg, C. Sagui, S. Schott-Verdugo, J. Shen, C. L. Simmerling, N. R. Skrynnikov, J. Smith, J. Swails, R. C. Walker, J. Wang, L. Wilson, R. M. Wolf, X. Wu, Y. Xiong, Y. Xue, D. M. York, and P. A Kollman, *AMBER 20* (University of California, San Francisco 2020).

[35]A. W. Sousa Da Silva and W. F. Vranken, "ACPYPE—AnteChamber PYthon Parser interfacE," BMC Res. Notes **5**(1), 367 (2012).

[36]A. Minoia, L. Chen, D. Beljonne, and R. Lazzaroni, "Molecular modeling study of the structure and stability of polymer/carbon nanotube interfaces," Polymer **53**(24), 5480–5490 (2012).

[37]M. Vögele, J. Köfinger, and G. Hummer, "Molecular dynamics simulations of carbon nanotube porins in lipid bilayers," Faraday Discuss. **209**, 341–358 (2018).

[38]M. J. Frisch, G. W. Trucks, H. B. Schlegel, G. E. Scuseria, M. A. Robb, J. R. Cheeseman, G. Scalmani, V. Barone, G. A. Petersson, H. Nakatsuji, X. Li, M. Caricato, A. V. Marenich, J. Bloino, B. G. Janesko, R. Gomperts, B. Mennucci, and D. J. Hratch, *Gaussian 16, Revision C.01* (Gaussian, Inc., Wallingford, CT, 2016).

[39]J. Wang, W. Wang, P. A. Kollman, and D. A. Case, "Automatic atom type and bond type perception in molecular mechanical calculations," J. Mol. Graph. Model. **25**(2), 247–260 (2006).

[40]J. Qi, N. Edirisinghe, M. G. Rabbani, and M. P. Anantram, "Unified model for conductance through DNA with the Landauer-Büttiker formalism," Phys. Rev. B **87**(8), 085404 (2013).

Published under an exclusive license by AIP Publishing